C. R. Physique 11 (2010) 457–471

Contents lists available at ScienceDirect

Comptes Rendus Physique

www.sciencedirect.com

Terahertz electronic and optoelectronic components and systems

Frequency-agile terahertz-wave generation and detection using a nonlinear optical conversion, and their applications for imaging

Systèmes de rayonnement térahertz, ajustables en fréquence, basés sur des effets optiques non linéaires, et leurs applications en imagerie

Hiroaki Minamide [a,*], Hiromasa Ito [a,b]

[a] *RIKEN Advanced Science Institute, 519-1399 Aramaki Aoba, Sendai, Miyagi, 980-0845, Japan*
[b] *Graduate School of Engineering, Tohoku University, Aramaki Aoba, Sendai, Miyagi, 980-8579, Japan*

ARTICLE INFO

Keywords:
Terahertz-wave parametric oscillation/generation
Difference frequency generation
Widely tunable source
Terahertz-wave detection
Nonlinear optical conversion
Carrier density mapping
Water concentration mapping

Mots-clés :
Oscillation/génération térahertz paramétrique
Génération par différence de fréquence
Génération très large bande
Détection des ondes THz
Conversion optique non linéaire
Carte de densité de charges libres
Carte de concentration aqueuse

ABSTRACT

We have developed widely tunable terahertz (THz)-wave sources using nonlinear optical crystals. In the 1–3 THz region, a frequency-agile THz-wave parametric oscillator in a ring-cavity configuration has been realized using MgO-doped $LiNbO_3$ as the nonlinear crystal. An organic 4-dimethylamino-N-methyl-4-stilbazolium tosylate (DAST) crystal is promising for THz-wave generation in an ultra-wide range 1–40 THz. Difference-frequency generation from DAST, pumped using a dual-wavelength $KTiOPO_4$ (KTP) optical parametric oscillator, is demonstrated. Additionally, THz-wave detection, with high sensitivity, fast response-time and room-temperature operation, is achieved by nonlinear up-conversion. Water concentration mapping of biological tissue samples and carrier density mapping of semiconductor wafers using frequency-agile THz-wave sources are demonstrated.

RÉSUMÉ

Nous avons développé des sources de rayonnement térahertz basées sur des techniques d'optique non linéaire, qui sont réglables sur une très large bande fréquentielle. Dans la région 1–3 THz, nous avons construit un oscillateur paramétrique comprenant un cristal non linéaire de $LiNbO_3$ dopé MgO au sein d'une cavité résonante en anneau. Pour la génération très large bande (1–40 THz), le cristal organique DAST (4-dimethylamino-N-methyl-4-stilbazolium tosylate) présente des performances très prometteuses. Ainsi, nous l'avons utilisé pour de la génération THz par différence de fréquence entre les 2 faisceaux délivrés par un oscillateur optique paramétrique en KTP ($KTiOPO_4$). De plus, la technique non linéaire de « *up-conversion* » permet une détection des ondes THz avec une extrême sensibilité et un temps de réponse très bref à température ambiante. En employant ces sources, nous avons enregistré des cartes de concentration aqueuse de tissus biologiques et des cartes de densité de charges libres dans des semi-conducteurs.

* Corresponding author.
E-mail address: minamide@riken.jp (H. Minamide).

1631-0705/$ – see front matter
doi:10.1016/j.crhy.2010.05.005

1. Introduction

During the 50 years since the first demonstration of the laser, many areas of laser science have been explored. Nonlinear optics is one of the fields that has been enabled by the laser. The development of nonlinear techniques has been extended into the terahertz (THz)-wave region. Many studies have been carried out concerning the generation of coherent THz-wave radiation [1–3]. Additionally, in recent years, the THz-wave region has proven to be very attractive in a range of activities, from the fundamental science to advanced applications for industry. Our research has focused on development of coherent, tunable THz-wave sources, covering a wide spectral range [4–8]. These sources are bridging the gap between broadband THz generation used in THz time-domain spectrometry systems (THz-TDS), and monochromatic generation such as quantum cascade lasers (QCLs).

In this article, we describe the development of frequency-agile THz-wave sources in the range 1–40 THz. We employ a THz-wave parametric oscillator using MgO-doped $LiNbO_3$ crystal in a ring-cavity configuration. To obtain wider tunability, an organic 4-dimethylamino-N-methyl-4-stilbazolium tosylate (DAST) was used. Also, difference-frequency generation using the DAST crystal pumped with a dual-wavelength $KTiOPO_4$ optical parametric oscillator (KTP-OPO) has been demonstrated. Practical applications using such a widely tunable monochromatic THz source require a suitable detection technique. A THz-wave detection system using nonlinear up-conversion and operating at room temperature is described. Water concentration mapping of biological tissue samples and carrier density mapping of a semiconductor wafer are demonstrated as applications of our tunable THz-wave sources.

2. Frequency-agile terahertz-wave sources

2.1. Ring-cavity THz-wave parametric oscillator

THz-wave generation in our sources is based on parametric down-conversion utilizing the polariton mode scattering of a $LiNbO_3$ nonlinear optical crystal. In this parametric process, frequency conversion occurs between the pump (ω_p) and idler (ω_i) beams at near-infrared frequencies and THz frequencies (ω_T) correspondingly. According to energy conservation $\omega_p = \omega_i + \omega_T$. Phase matching of the wave vectors of the pump, $\mathbf{k}_p$, idler, $\mathbf{k}_i$, and THz, $\mathbf{k}_T$, beams is satisfied under the conservation of momentum noncollinearly, i.e., $\mathbf{k}_p = \mathbf{k}_i + \mathbf{k}_T$. The frequency can be tuned by varying the phase-matching angle between the idler and pump beams. In our system, the angle can be varied over a range of 1–3 degrees.

We have developed THz-wave parametric sources using this generation technique, including THz-wave parametric oscillators (TPOs) with a linear cavity [4–8] and THz-wave parametric generators (TPGs) without any cavity [9–11]. These sources have several features that make them superior to other THz-wave sources. They are highly coherent, have high-output power, are compact and operate at room-temperature. Another advantage of these tunable THz-wave sources is frequency agility, which allows fast frequency tunability and random frequency access. This feature is significant for many applications, such as monitoring rapid phenomena, measuring frequency-rationed images, and the rapid acquisition of spectroscopic data.

To obtain a frequency-agile THz-wave source operating at room temperature, we proposed a ring-cavity TPO with a novel, simple tuning mechanism [12,13]. Frequency tuning was obtained by controlling the rotation of a mirror installed in the idler cavity. This allowed rapid control of the frequency. Also, using a ring-cavity configuration is an effective method of obtaining high oscillation stability.

Fig. 1 shows the optical arrangement. To achieve THz-wave frequency tuning the angle of the mirror labeled M_3 can be controlled using a Galvano-optical beam scanner (Harmonic Drive Systems, LSA-20B-30-SP). Point P in the cavity is assumed to lie on the idler path of the cavity and remains fixed when the path of the idler beam is changed during tuning. From the figure, it can be seen that the various idler paths from P_1 to P_2 are conceivable for any point of reflection on M_3. In the geometrical optics description, only a single path is selected for any arrangement. Therefore, the phase-matching angle can be varied by controlling the angle of M_3 and THz-wave frequency tunability can be obtained.

Fig. 2 shows a photograph of the experimental setup used. The ring cavity consisted of three mirrors (M_1, M_2, and M_3) for the idler beam (>1.067 μm). Mirror M_2 was a general high-reflectance (HR) mirror. However, this experiment introduced super-mirrors (Optoquest) to separate the pump (1.064 μm) and idler beams. Because the phase-matching angle was varied from 1 to 3 degrees, it was difficult to separate the two beams spatially. Super-mirrors provide steep transmittance characteristics: ~ 0 dB at 1.064 μm, -2 dB at 1.067 μm, and less at longer wavelengths, when the incident angle of the idler beam is 30 degrees.

The distances between the centers of the mirror surfaces, i.e., M_1–M_2, M_1–M_3, and M_2–M_3, were set to 100, 97, and 103 mm, respectively. The response time of the Galvano-optical scanner was around 1 ms per degree, which corresponds to about 1 ms per THz. The angle was controlled from a computer via a digital–analog converter board (NI, DAQcard-6024E), which controls the voltage at the beam scanner. A 5 mol% MgO-doped $LiNbO_3$ crystal, 63 mm long, 4 mm wide and 5 mm high, was used as the nonlinear optical crystal. The x-surfaces at both ends were mirror polished and coated with antireflection coating centered at 1.064 μm. The y-surface was also polished to minimize the coupling gap between the Si prism base and the crystal surface, and to prevent scattering of the pump beam, which excites free carriers at the Si prism base. An array of six Si prism couplers was placed on the y-surface of the crystal for efficient coupling of the THz wave [14]. The 1.064-μm pump source used in this experiment was an LD-pumped Q-switched Nd:YAG laser developed in collaboration with the RIKEN Teraphotonics team and MegaOpto. The pulse width was 17 ns when the output power was

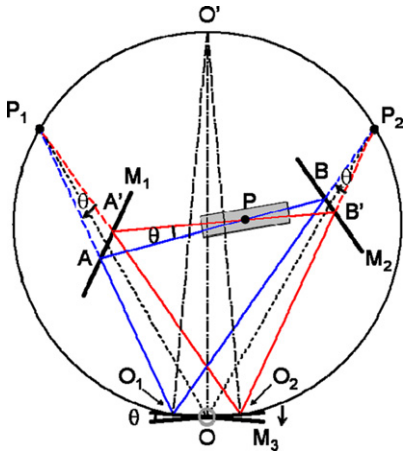

Fig. 1. Schematic illustration of the principal of the idler tuning. The three-mirrored cavity for the idler beam consists of mirrors M_1, M_2, and M_3. M_1 and M_2 are fixed mirrors, whereas M_3 is mounted on a Galvano-optical beam scanner and is movable in the angular direction. Point P in the cavity is assumed to lie on the idler path of the cavity and remains fixed when the path of the idler beam is changed during tuning. Points P_1 and P_2 are images of P in mirrors M_1 and M_2, respectively.

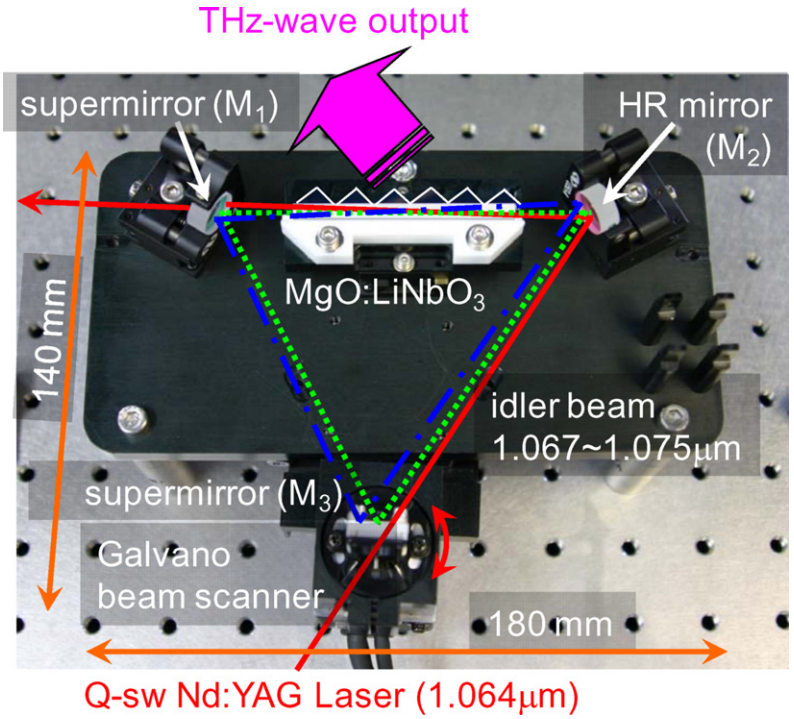

Fig. 2. Photograph of the ring-cavity THz-wave parametric oscillator. The supermirror can separate the idler beam (1.067–1.075 μm) from the pump beam (1.064 μm).

20 mJ/pulse, and the maximum repetition rate was 500 Hz. Using a high-repetition-rate pump laser, rapid frequency tuning and fast random frequency switching were possible with the ring-cavity TPO.

Fig. 3 shows the THz-wave output as a function of the frequency and the relationship between the THz-wave frequency and the control voltage applied to the scanner. A 4.2-K a liquid-helium-cooled Si bolometer was used to detect the THz-wave radiation. Output powers of approximately 6 nJ/pulse were obtained in the range 1.3–1.6 THz. The minimum direct-detection of THz radiation without conventional high-sensitivity electrical detection (i.e., a lock-in amplifier) was about 0.84 pJ/pulse. Consequently, a frequency tuning range from 0.93 to 2.7 THz was obtained.

To evaluate the performance of the ring-TPO, a rapid spectroscopic imaging experiment was performed [15]. Images of both homogeneously and inhomogeneously mixed samples were extracted using a multivariate regression analysis [16]. The samples included glucose, maltose, and polyethylene in form of pellets. Each pure sample has different absorption peaks, as shown in Fig. 4. Principle component analysis was used to identify the samples based on spectral peaks of the

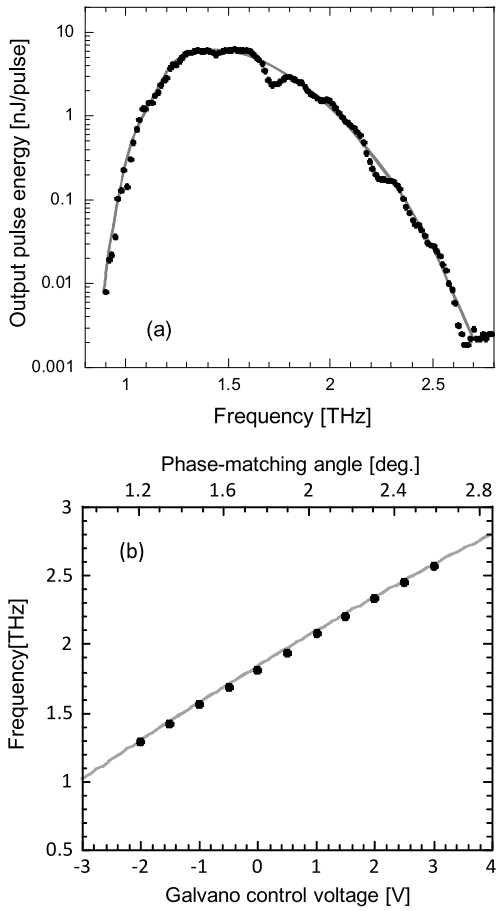

Fig. 3. (a) THz-wave output power as a function of frequency. (b) Relationship between the frequency of the THz radiation and the applied control voltage to Galvano-optic scanner.

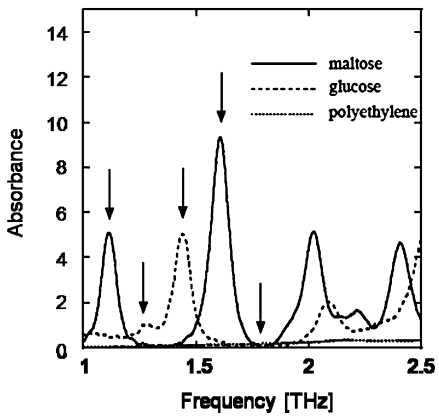

Fig. 4. Absorption spectra of maltose, glucose, and polyethylene. The arrows indicate the absorbance data sets of five different wavelengths used for principle component analysis.

pure substances. The multi-wavelength imaging was obtained by controlling the THz wave periodically at these discrete wavelengths. A scanning rate of 500 Hz was used, and the component analysis was performed simultaneously.

Fig. 5(a) shows THz images of the homogeneous samples. The estimated concentrations of glucose and maltose from the principle component analysis were $12.1 \pm 2.5\%$ and $12.0 \pm 2.0\%$, respectively, which is within 10% of the composition of the samples. Images of the inhomogeneous samples are shown in Fig. 5(b). These patterns were reproducible and corresponded to the spatial variation in concentration of the samples. From these data, it was found that sugar compounds with concen-

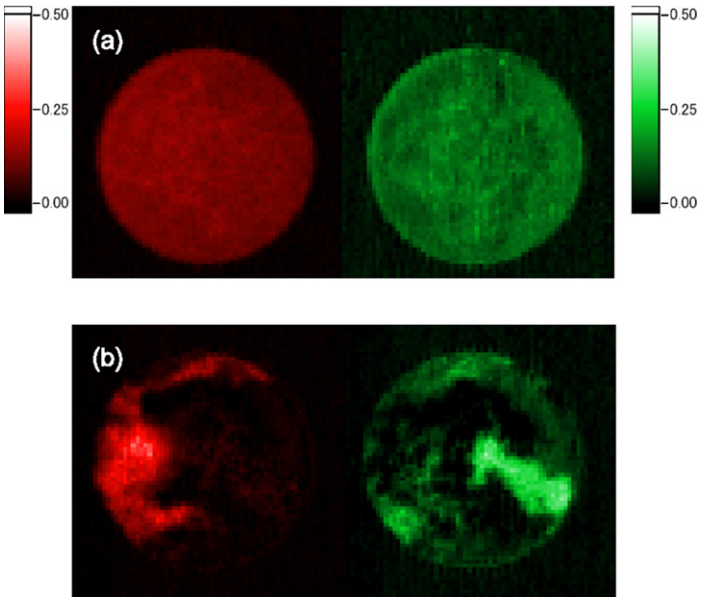

Fig. 5. (a) Concentration patterns of glucose (left) and maltose (right) in a homogeneously mixed pellet. (b) Concentration patterns of glucose (left) and maltose (right) in an inhomogeneously mixed pellet.

trations of less than 5% by weight could be easily detected. It took less than 4 min to measure the multi-wavelength image, including the principle component analysis, for a scanning area of 16.25 × 16.25 mm (65 × 65 pixels).

2.2. DAST-DFG THz-wave source

Among methods of THz-wave generation using nonlinear optical down-conversion, difference-frequency generation (DFG) is the most promising. It allows wide tunability and high-power output. An organic nonlinear optical crystal, 4-dimethylamino-N-methyl-4-stilbazolium tosylate (DAST), developed by Nakanishi et al. [17], is an excellent material for efficient and high intensity THz-wave generation because of its large second-order optical nonlinearity ($d_{11} = 230$ pm/V). This value is about 10 times larger than that of conventional inorganic materials for THz-wave generation, such as $LiNbO_3$. In addition, the refractive index of DAST at optical frequencies is almost the same as it is at THz frequencies. Therefore, collinear DFG phase matching of type 0 (the polarization of all waves in nonlinear wavelength conversion are parallel) can be achieved without using birefringent phase matching or quasi-phase matching.

Typically, organic nonlinear optical crystals have large optical nonlinearity. However, in many cases, it is too difficult to grow sufficiently large crystals of high quality because of the morphology and thermal decomposition behavior in the liquid state. We have identified favorable growth conditions of DAST and have been able to reproducibly grow large crystals about 10 mm^2 in area, as shown in Fig. 6(a).

In order to realize effective and widely tunable THz-wave generation using the DAST-DFG source, the optimum phase-matching condition should be satisfied [18]. Fig. 6(b) shows the results of calculated coherence length distribution in DAST-DFG based on the type 0 phase-matching condition. Coherence length greater than 1 mm can be achieved. THz-wave generation using DAST-DFG can be achieved by an independently controlled dual-wavelength pump source in the range 1.3–1.6 μm.

Fig. 7 shows a schematic diagram of the frequency-agile, ultra-widely tunable DAST-DFG THz-wave source [19]. A double-crystal KTP optical parametric oscillator was developed as an independently controlled dual-wavelength pump source. The two KTP crystals were positioned in opposite orientations to stabilize the beam position and minimize the walk-off. The angle of the KTP crystals was controlled using the Galvano-optical scanner. The crystals were mounted on scanners inside a linear OPO resonator (formed by mirrors M_1 and M_2, as shown in Fig. 7) to form a simple flat–flat type II OPO. The dual-wavelength output of the KTP-OPO was focused into the DAST crystal. The emitted THz-wave was collimated using a gold off-axis parabolic mirror (254-mm focal length) and focused onto a pyroelectric detector using another off-axis parabolic mirror.

The pump beam and stray light were shielded from the detector using a Yoshinaga filter and black polyethylene filter. The THz-wave output power variation with frequency is shown in Fig. 8. The wavelength of the pump, λ_1, was controlled within the range 1.3–1.58 μm using the Galvano scanner, the wavelength of idler, λ_2, was fixed at 1.3 μm, and the DAST crystal remained fixed. The pump power was around 2 mJ/pulse. DAST-DFG THz-wave generation was obtained in the range 1–40 THz.

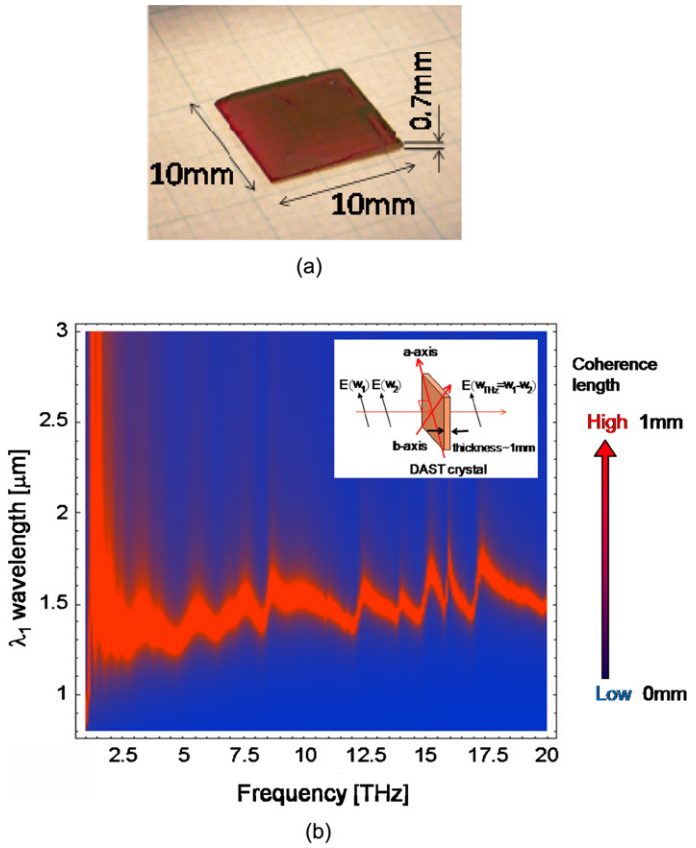

Fig. 6. (a) Photograph of a DAST crystal and the calculated coherent length distribution of DFG. (b) The vertical axis is the wavelength of two pump beams and the horizontal axis is the frequency of the THz-wave radiation. The inset shows the arrangement of pump beams, THz-wave beam, and the DAST crystal.

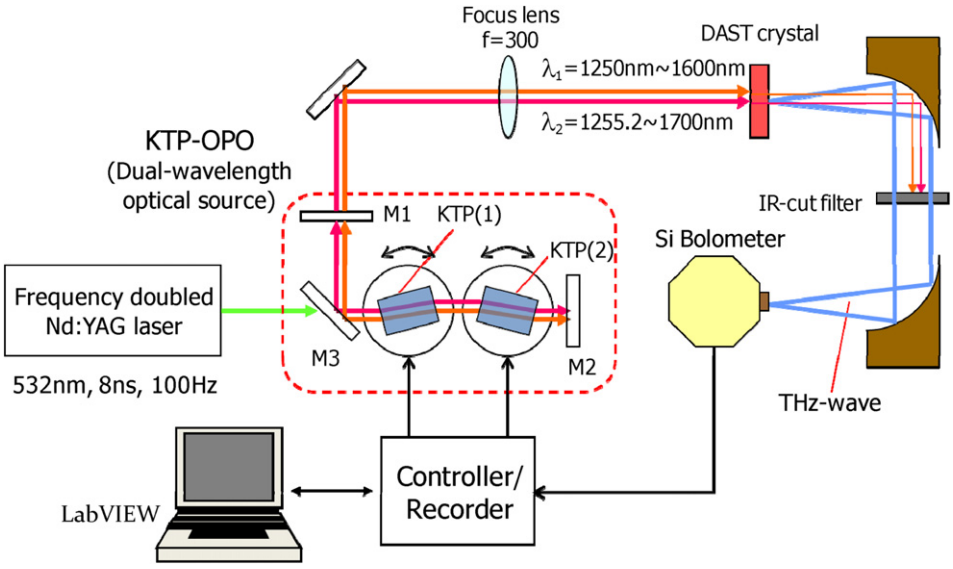

Fig. 7. Experimental setup of DAST-DFG THz-wave source, which is pumped using a dual-wavelength KTP-OPO.

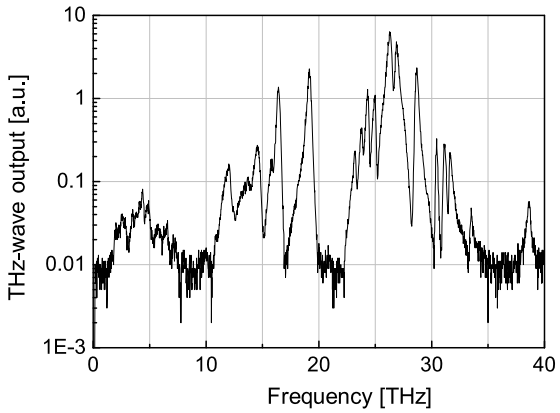

Fig. 8. THz-wave output as a function of THz frequency in DAST-DFG.

The DAST crystal has potential for more wideband THz generation [20]. In this experiment, THz-wave generation was limited to < 40 THz by the dual-wavelength KTP-OPO pump. Wider tunability could be achieved by using a more widely tunable source as the pump.

3. THz-wave detection using nonlinear optical up-conversion

Practical applications using such a widely tunable monochromatic THz source have been impeded by the lack of suitable detection for operation at room temperature. One of the most sensitive and most common THz detectors available so far is a bolometer. Monochromatic THz-wave radiation is generally measured using a liquid-helium-cooled Si bolometer. The bolometer also has a slow response, with a time constant of several hundred microseconds. However, room-temperature direct THz-wave detectors such as pyroelectrics and Golay cells offer poor sensitivity. A new detection technique is therefore required.

Optical detectors in the near-IR/visible region offer excellent performance with very high efficiencies, low noise equivalent power (NEP), and large bandwidths and can operate at room temperature. Thus, if it were possible to convert THz-wave radiation to visible or near-IR radiation, then in principle, more sensitive detection would be possible.

Several studies into frequency up-conversion of THz radiation and detection of the up-converted IR signal have been performed [21,22]. We propose THz-wave radiation detection using frequency up-conversion and parametric amplification in nonlinear MgO:$LiNbO_3$ crystals [23]. This involves mixing THz-wave radiation with an intense near-IR pump beam to generate light at a difference frequency due to the stimulated polariton scattering process. This difference frequency up-converted signal is then amplified using a MgO:$LiNbO_3$ optical parametric amplifier and allows for high-sensitivity detection. The intensity of the up-converted signal is proportional to that of the incident THz-wave radiation, and it preserves also the phase information of the THz signal. The THz-wave radiation parameters can then be extracted from the up-converted radiation and detected using an InGaAs-based photodiode.

Fig. 9 shows a schematic diagram of the experimental setup for room temperature detection of monochromatic THz-wave pulses. The THz-wave radiation was generated by an injection-seeded THz-wave parametric generator (is-TPG). The pump beam was provided by a single-mode Q-switched Nd:YAG laser, the same source that we used to pump the is-TPG.

The nonlinear detection system consisted of two parts: the input coupling crystal and the parametric amplifying crystal. The input coupling crystal was an equilateral trapezoid. The THz-wave radiation from the is-TPG was incident normal to the longer side of the parallel surfaces of the crystal. The pump beam was incident normal to one of the beveled edges, and total reflection occurred at the longer side of the parallel surfaces. Mixing the THz-wave signal with the intense pump pulse at the input of the detector crystal created a narrow-line-width difference-frequency up-converted signal. This up-converted signal was parametrically amplified by the 130-mm-long MgO:$LiNbO_3$ optical parametric amplifier crystal to achieve highly sensitive detection. Two specially manufactured edge filters were used to separate the amplified up-converted beam from the pump beam. The up-converted signal was separated from the pump laser and then detected using a high-speed InGaAs *p-i-n* photodiode, which was connected to a fast digital oscilloscope to capture the temporal profile of the up-converted signal.

Fig. 10 shows the measured temporal profiles of the up-converted signal at different incident THz-wave powers. The background noise was recorded by blocking the injected THz-wave beam with a transparent glass plate; the noise is from residual pump scattering and parametric fluorescence. Our experiment demonstrates that the MgO:$LiNbO_3$ detector is able to detect THz-wave signals with sensitivity at least one order of magnitude greater than a typical Si bolometer.

The pulse width for the THz-wave signal was 4.7 ns, determined from the temporal profile of the up-converted signal. Therefore, our detector is capable of capturing the temporal profiles of nanosecond-long THz pulses, whereas a Si bolometer has a much slower response, with a time constant of approximately 300 μs, and therefore gives the average power of a THz pulse only.

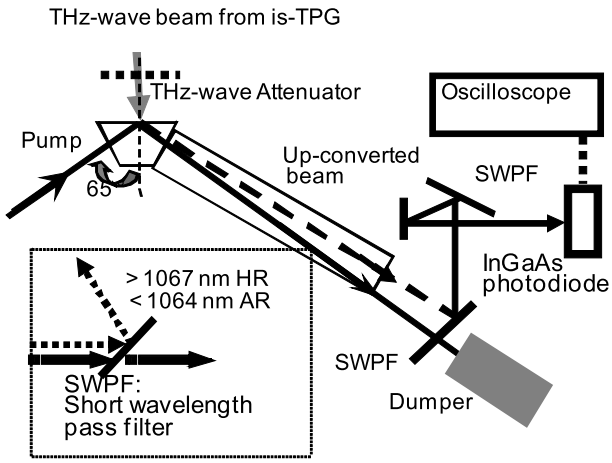

Fig. 9. Schematic diagram showing the experimental setup of the THz-wave detection using a MgO:$LiNbO_3$ crystal. Two specially manufactured edge filters were used to separate the amplified up-converted beam from the pump beam.

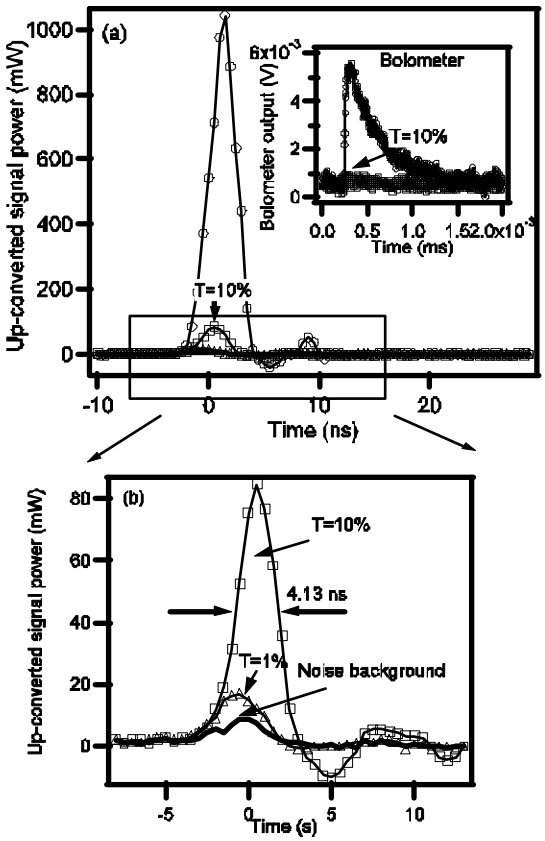

Fig. 10. (a) The measured temporal profiles of the up-converted signal for different incident THz-wave intensities. The inset shows the bolometer measurements of the THz-wave radiation prior to entering the nonlinear crystal. The $T = 10\%$ and $T = 1\%$ annotations refer to measurements of the temporal profiles of THz-wave radiation and the up-converted signal by inserting THz-wave attenuators of 10% or 1% transmittance, respectively; (b) shows a close-up of the region illustrated by the box in (a). The thick black line in (b) was recorded by blocking the injected THz-wave beam with a transparent glass plate.

Balanced homodyne detection (BHD) was employed for phase detection. The idler beam from the is-TPG was employed as a local oscillator to provide a phase reference for BHD. Fig. 11 shows the interference signal as a function of the relative path-length difference of the THz-wave beam. Consequently, we demonstrated THz-wave phase detection as well as amplitude detection using frequency up-conversion.

In order to cover the ultra-wide tuning range of DAST-DFG, we developed highly sensitive, fast-response THz-wave detection employing a DAST crystal that operated at room temperature [24]. Fig. 12 shows the experimental setup of the

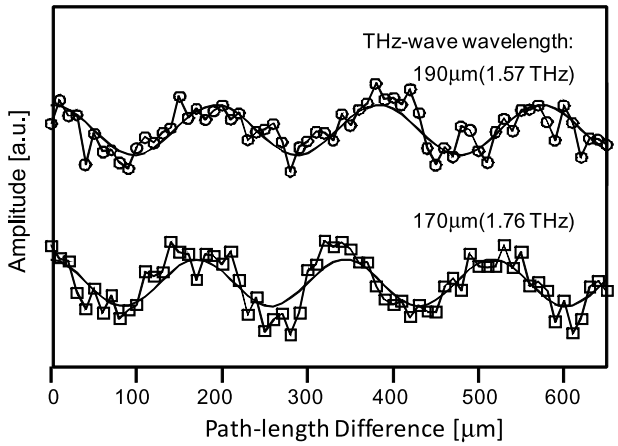

Fig. 11. The measured interference signal as a function of the relative path-length difference of the THz-wave beam

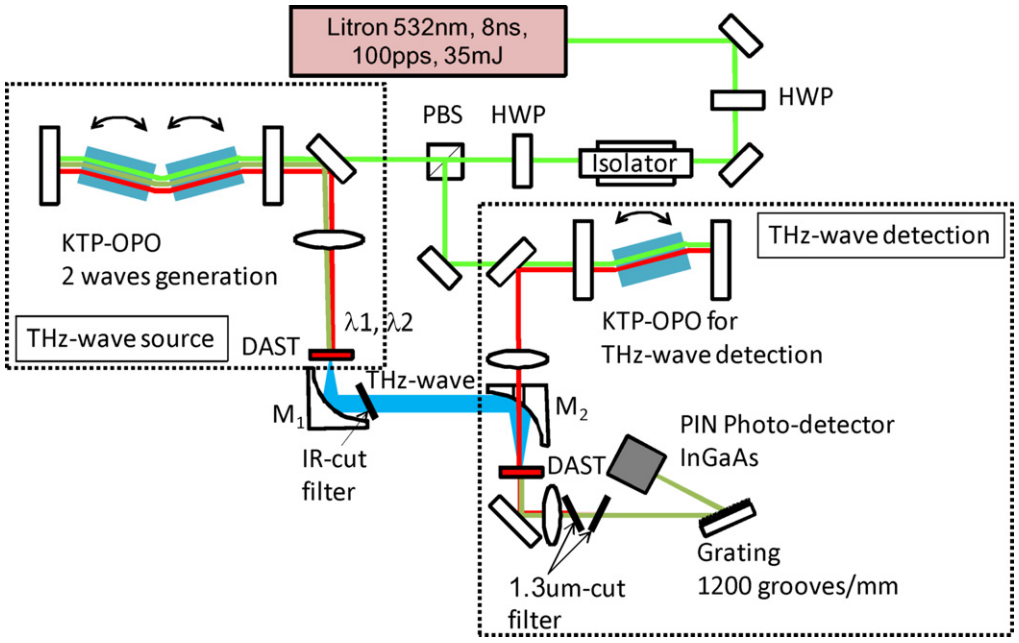

Fig. 12. Experimental setup of THz-wave generation and THz-wave detection using DAST crystals.

THz-wave generation and detection system. The pump was a pulsed 532-nm signal from the second harmonic of a 1064-nm Q-switched Nd:YAG laser (8 ns, 100 pps, 35 mJ/pulse). The ultra-wide tunable THz-wave source consisted of a DAST crystal and a dual-wavelength KTP-OPO. The pump beam was split using a polarized beam splitter to pump two KTP-OPOs. One KTP-OPO is the pump for THz-wave generation, and the other one is for detection. The splitting ratio was controlled by rotating the linear polarization of the pump beam with a half-wave plate.

The 1.3-μm radiation from the second KTP-OPO passed through an aperture in the parabolic mirror M_2 and irradiated the DAST crystal used for the pump beam. The THz-wave radiation generated was directed through a low pass filter to remove the IR radiation and was reflected at the parabolic mirror M_2. Finally, the THz-wave beam was focused on to the detection DAST crystal.

When the THz-wave radiation was incident on the detection DAST, an IR signal beam was generated through nonlinear up-conversion. Fig. 13 shows a temporal variation of the 1.42-μm up-converted signal (corresponding to 19.3 THz). To check if the signal is due to up-conversion of the THz-wave signal, we measured the photodetector output when the THz-wave beam was blocked.

No signal was observed when the THz-wave radiation was not incident on the second DAST crystal. Consequently, we can conclude that the response of the photodetector was due to the THz-wave input. The up-converted signal was coupled into an optical fiber, and the spectrum was measured using a compact spectrometer. The spectra of IR signals corresponding to THz-wave signals of 16, 19, and 26 THz are shown in Fig. 14 [25].

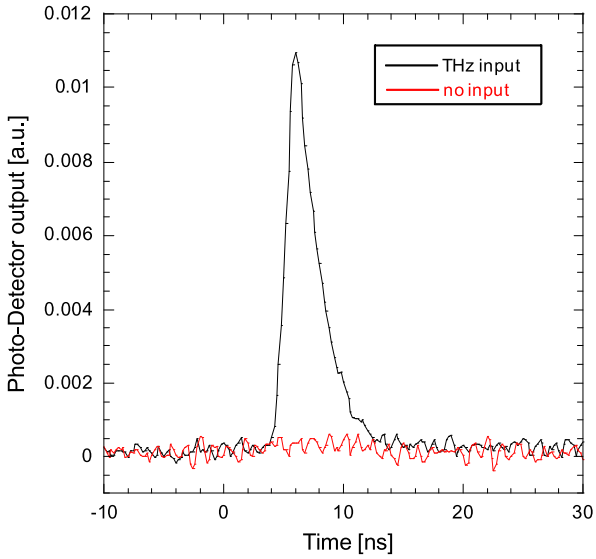

Fig. 13. The temporal evolution of the up-converted signal.

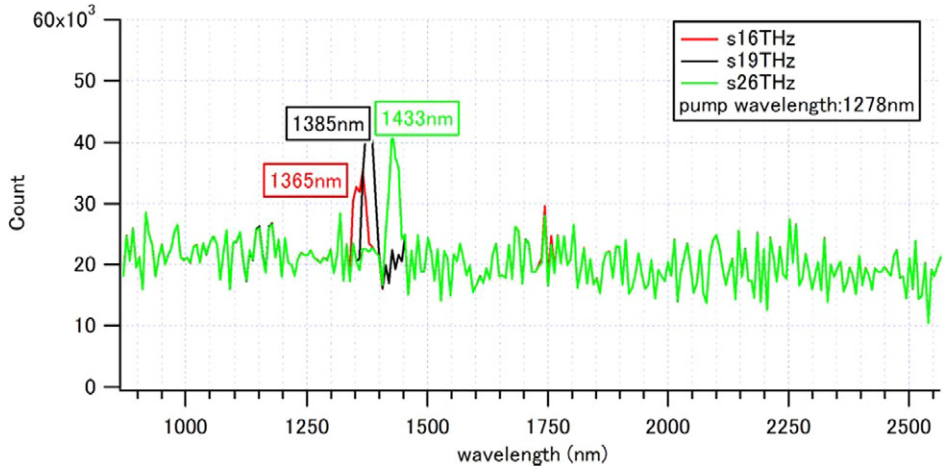

Fig. 14. Spectra of the up-converted signals corresponding with to THz-wave radiation at 16, 19, and 26 THz.

4. THz applications of frequency-agile THz-wave sources

4.1. Water concentration mapping of biological tissue

THz radiation is strongly absorbed by water. This provides potential for measuring the water content of a sample. Knowledge of the water content can provide important information in the field of biology. For example, most pathological changes in the liver are known to increase the amount of free water content.

We proposed a water-content measurement method using a tunable THz-wave source and demonstrated two-dimensional water-level mapping in thin biological tissue samples [26]. Fig. 15 shows the absorption coefficient of pure water and of human liver tissue without water. The absorption coefficient of water is much higher than that of the tissue. We assume that the absorption in fresh tissue is due to the water it contains, and use the Lambert–Beer law to relate the transmittance, T, to volume fraction of water, v_w:

$$T \approx e^{-(\alpha_w v_w)d}, \tag{1}$$

where α_w is the absorption coefficient of the water, and d is the sample thickness. The maximum sensitivity is obtained when $\alpha_w v_w d = 1$. Fig. 16 shows the calculated sample thickness as a function of the water volume concentration to achieve maximum sensitivity. The maximum sensitivity is obtained with a transmittance of 36.8%. Considering that the absorption coefficient of water is in the range 200–1400 cm^{-1}, the optimal sample thickness should be in the range 10–200 μm.

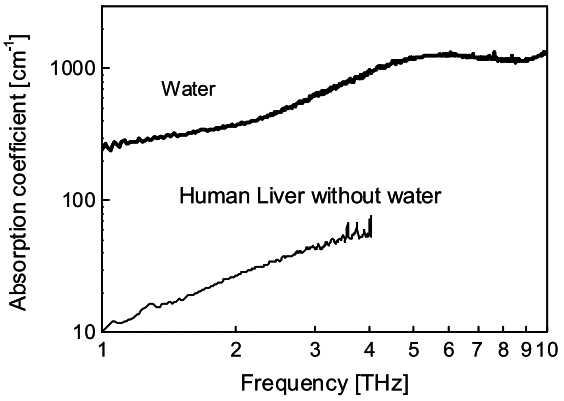

Fig. 15. Absorption coefficients of pure water and human liver tissue without water.

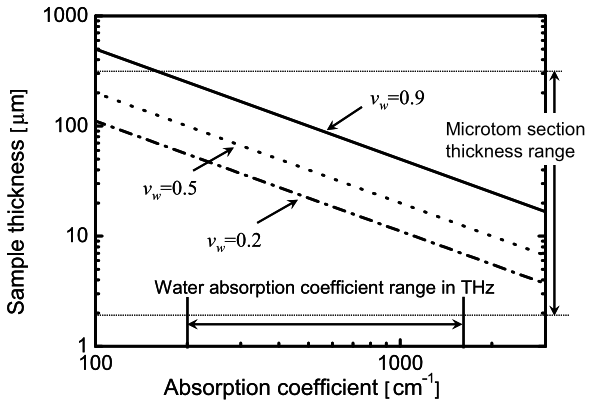

Fig. 16. Relationship between the absorption coefficient and sample thickness, satisfying the high sensitivity condition: $\alpha_w v_w d = 1$. The moderate thickness range is 10–200 μm, considering a water absorption coefficient of 200–1400 cm^{-1}.

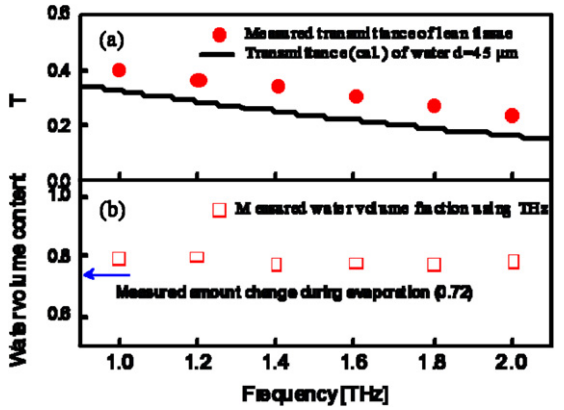

Fig. 17. (a) Measured transmittance of porcine muscle tissue and the calculated transmittance of water. (b) Measured water volumetric fraction of water using the THz measurement system and by measuring the difference in mass following dehydration.

Biological samples with a thickness in the range 5–250 μm can be prepared using a microtome, which covers the optimal thickness range of our measurement technique.

Fig. 17(a) shows the frequency dependence of transmittance of a 45-μm-thick sample of porcine muscle tissue. The transmittance is monotonic, and the trend is similar to that of water, indicating that the water is the primary contributor to the absorption in the THz frequency range. This monotonic change in the transmittance makes it possible to control the maximum sensitivity according to Lambert–Beer's law by choosing the frequency. Fig. 17(b) shows the measured water volumetric fraction using the THz measurement system operating in the range 1.0–2.0 THz. The relative error between the THz-wave method and mass loss following dehydration was less than 10%.

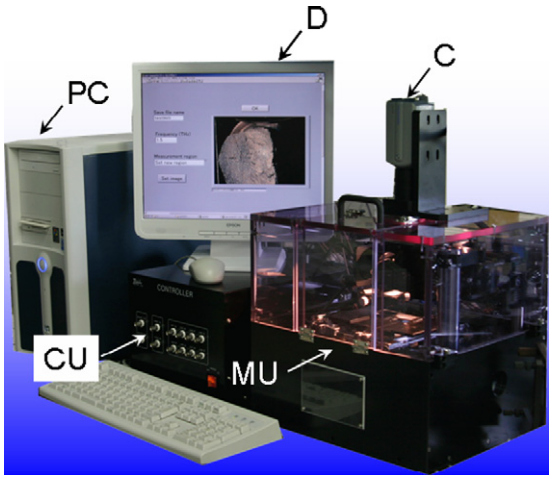

Fig. 18. Photograph of the measurement system. The system comprises a main optical unit (MU), a CCD-array camera for the sample monitor (C), a control unit for sample stages and signal processing (CU), a computer (PC), and a display (D). The THz-wave source is not included in this photograph.

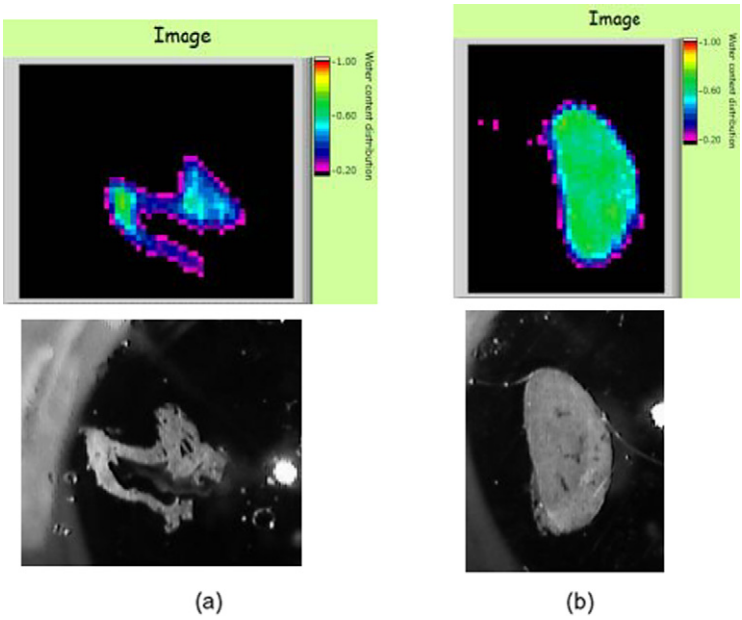

Fig. 19. Water content distribution of sampled of (a) lung tissue from a mouse and (b) kidney tissue from a mouse using the THz transmission method. The upper figures show the water distribution, and lower figures show photographs of the samples.

We developed a THz-wave spectroscopic imaging system using the ring-TPO, as shown in Fig. 18. This system included a main measurement unit and a specially developed control unit. The main measurement unit includes several THz mirrors, aspherical lenses, a sample-mount XY stage, and a CCD-array camera and is computer-controlled. The small size of 3λ (λ: THz wavelength) is achieved using a specially designed aspherical lens: a Tsurupica lens. The control unit includes an analog-to-digital converter and a stage driver for sample scanning. The sample is observed using a CCD-array camera, and the area for THz image acquisition is selected on the display. The subsequent measurement is then automated.

The biological samples for two-dimensional water mapping were sliced to 60-μm thickness using a microtome (LEICA 1900CM). The samples were immersed/blocked in oleic acid to avoid water evaporation. Fig. 19(a) shows the measured water content distribution of a sample of lung tissue taken from a mouse, and Fig. 19(b) shows a sample from a mouse kidney. The shape of the samples can be clearly seen.

4.2. Carrier density mapping of semiconductor wafer

Many of the physical properties of semiconductors are affected by the density of carriers. Hall measurements are traditionally used to obtain the carrier density information; however, it is difficult to measure the density distribution at a

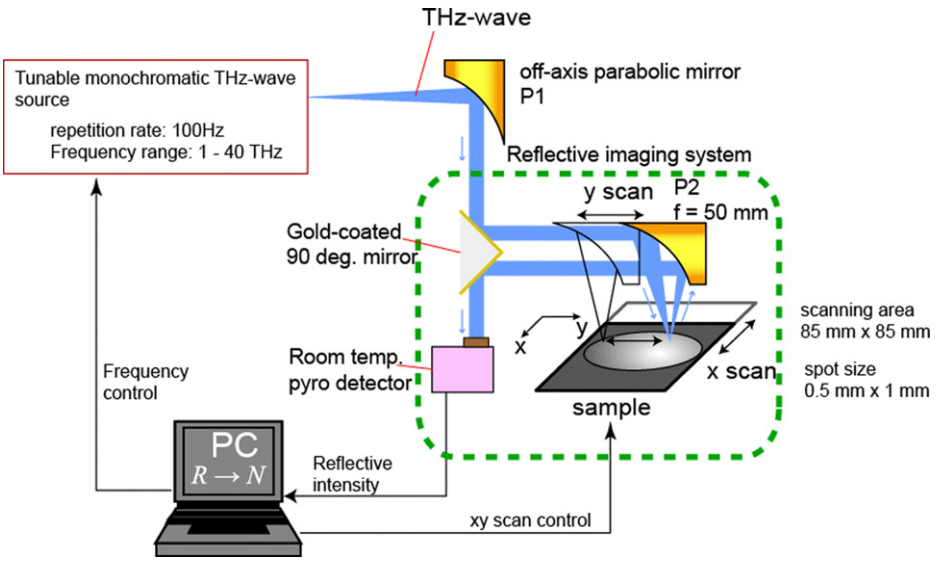

Fig. 20. Schematic diagram showing the experimental setup of the THz reflection measurement of the carrier density in a semiconductor wafer using a DAST-DFG THz source.

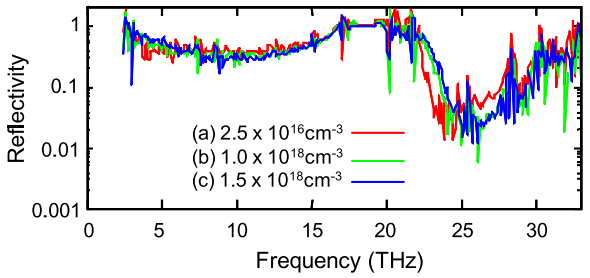

Fig. 21. THz reflective spectrum of GaN substrates with carrier densities of (a) 2.5×10^{16} cm^{-3}, (b) 1.0×10^{18} cm^{-3}, and (c) 1.5×10^{18} cm^{-3}.

surface, as it requires to make many electrical contacts. Knowledge of the carrier density obtained in a nondestructive manner is important not only for fundamental physics, but also for industrial applications. Because THz radiation reflectivity/absorption depends on the carrier density we have developed a nondestructive method for the carrier density distribution measurements in semiconductors, using the ultra-widely tunable THz-wave sources (i.e., 1–40 THz) [27].

When the THz-wave signal is close in frequency to the transverse optical phonon frequency, ω_{TO}, and the optical longitudinal phonon, ω_{LO}, the reflectivity $R(\omega \sim \omega_{TO})$ does not depend on the carrier density, N, because the optical phonon–THz-wave interaction is dominant. We used THz radiation in this frequency region ($\sim \omega_{TO}$) as a reference for the reflectivity measurement. The reflectivity away from this region, i.e., $R(\omega \neq \omega_{TO})$, is used for measuring N. Frequency agility and wide tunability are required for a THz-wave source to perform rapid measurements comparing the reflectivity for THz-wave at $\omega \sim \omega_{TO}$ and $\omega \neq \omega_{TO}$.

Fig. 20 shows a schematic diagram of the experimental setup. A frequency-agile dual-wavelength KTP-OPO was used for collinear THz difference-frequency generation. The KTP-OPO is tunable within 1250–1700 nm, enabling phase-matched THz-wave generation over a wide range. The idler from the KTP-OPO is focused on a polished DAST crystal (Furukawa Co., Ltd.), and THz-wave radiation is generated from the DAST crystal. The THz beam is collimated using an off-axis parabolic mirror and fed into a reflective imaging system. For mapping the reflective signal, the position of an off-axis parabolic mirror was controlled, and the sample stage was scanned, as shown in Fig. 20. The size of the scanning area was 85×85 mm. The reflected THz beam was detected using a pyroelectric detector operated at room temperature. The spatial resolution was estimated to be 2 mm, using a measurement of a reflective image for a line and space in this experiment.

Samples of GaN wafers with carrier densities of 2.5×10^{16}, 1.0×10^{18}, and 1.5×10^{18} cm^{-3} were used. The reflectance spectra, measured in the center of GaN wafers, are shown in Fig. 21. We mapped the THz reflected intensity for all the samples at 19.2, 22.7, and 26.5 THz. We used the map in 19.2 THz as a reference of the reflected intensity, as the carrier density has no effect on the reflectivity at this frequency.

Normalized reflectance images for 22.7 and 26.5 THz were obtained and are shown in Fig. 22. The reflectance intensities at 22.7 or 26.5 THz differ among samples, and the reflectivity is dependent on the carrier density in samples. Although this

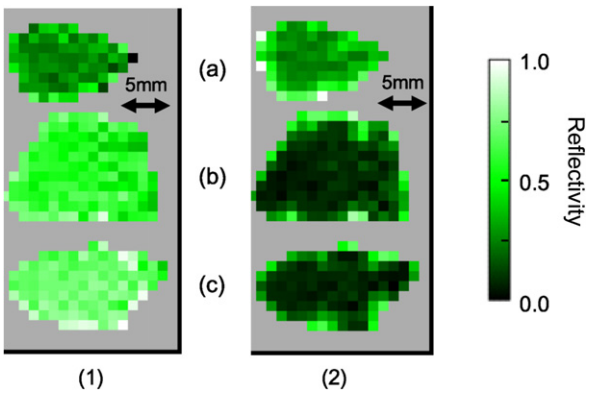

Fig. 22. Reflective images in three GaN wafers. Panels (1) and (2) show images for 22.7 and 26.5 THz, respectively, normalized by the reflected intensity at 19.2 THz.

technique necessitates further quantitative studies, we demonstrated an ability to distinguish between different levels of doping by a nondestructive measurement.

5. Conclusions

We have developed widely tunable THz-wave sources using nonlinear optical conversion. The $LiNbO_3$-based ring-TPO covers the range 1–3 THz. Using DAST-DFG results in a tunable THz source from 1 to 40 THz. We have developed THz-wave detection systems using nonlinear optical up-conversion. We demonstrated the use of $MgO:LiNbO_3$, highly sensitive, coherent THz-wave detection with fast response times at room temperatures. THz-wave detection using DAST allowed this to be extended to a wider frequency range.

We applied our THz-wave systems to water content mapping in biological samples and carrier-density mapping in semiconductor wafers. We expect that presented in this work monochromatic, frequency-agile and room-temperature operating THz-wave generation and detection methods will facilitate the further development of applications-oriented THz measurement in the near future.

Acknowledgements

The authors thank R. Guo, K. Miyamoto, T. Ikari, S. Ohno, and J. Zhang of RIKEN for their contributions, and S. Aiba (Tohoku Univ.) for sample preparation and discussion. Also, we would like to thank C. Takyu (Tohoku Univ.), T. Shoji (RIKEN), K. Akiyama (Mitsubishi Electric Co.) and A. Kudo (PAX Co.) for their technical assistance.

This work was partly supported by a Grant-in-Aid for Scientific Research (A) (No. 19206009) from the Japan Society for the Promotion of Science (JSPS).

References

[1] F. Zernike, P.R. Berman, Generation of far infrared as a difference frequency, Phys. Rev. Lett. 15 (1965) 999–1001.
[2] T. Yajima, K. Inoue, Submillimeter-wave generation by optical difference-frequency mixing of ruby R1 and R2 laser lines, Phys. Lett. A 26 (1968) 281.
[3] M.A. Piestrup, R.N. Fleming, R.H. Pantell, Continuously tunable submillimeter wave source, Appl. Phys. Lett. 26 (1975) 418–421.
[4] K. Kawase, M. Sato, T. Taniuchi, et al., Coherent tunable THz-wave generation from $LiNbO_3$ with monolithic grating coupler, Appl. Phys. Lett. 68 (1996) 2483–2485.
[5] J. Shikata, K. Kawase, M. Sato, et al., Characteristics of coherent terahertz wave generation from $LiNbO_3$ optical parametric oscillator, Electron. Comm. Jpn. Part II, Electronics 82 (1999) 46–53.
[6] K. Kawase, M. Sato, K. Nakamura, et al., Unidirectional radiation of widely tunable THz wave using a prism coupler under noncollinear phase matching condition, Appl. Phys. Lett. 71 (1997) 753–755.
[7] K. Imai, K. Kawase, H. Ito, A frequency-agile terahertz-wave parametric oscillator, Opt. Express 8 (2001) 699–704.
[8] T. Ikari, X.B. Zhang, H. Minamide, et al., THz-wave parametric oscillator with a surface-emitted configuration, Opt. Express 14 (2006) 1604–1610.
[9] K. Imai, K. Kawase, J. Shikata, et al., Injection-seeded terahertz-wave parametric oscillator, Appl. Phys. Lett. 78 (2001) 1026–1028.
[10] R.X. Guo, K. Akiyama, H. Minamide, et al., All-solid-state, narrow linewidth, wavelength-agile terahertz-wave generator, Appl. Phys. Lett. 88 (2006) 091120.
[11] A. Sato, K. Kawase, H. Minamide, et al., Tabletop terahertz-wave parametric generator using a compact, diode-pumped Nd:YAG laser, Rev. Sci. Instrum. 72 (2001) 3501–3504.
[12] H. Minamide, K. Kawase, K. Imai, et al., in: Conference on Lasers and Electro-Optics, OSA Technical Digest, Optical Society of America, Washington, D.C., 2001, p. 425.
[13] H. Minamide, T. Ikari, H. Ito, Frequency-agile terahertz-wave parametric oscillator in a ring-cavity configuration, Rev. Sci. Instrum. 80 (2009) 123104-1–123104-5.
[14] K. Kawase, J. Shikata, H. Minamide, et al., Arrayed silicon prism coupler for a terahertz-wave parametric oscillator, Appl. Opt. 40 (2001) 1423–1426.
[15] K. Akiyama, H. Minamide, H. Ito, Spectroscopic imaging with a ring-cavity THz-wave parametric oscillator, in: 13th Coherent Laser Radar Conference, 2005, pp. 214–217.

[16] Y. Watanabe, K. Kawase, T. Ikari, et al., Spatial pattern separation of chemicals and frequency-independent components by terahertz spectroscopic imaging, Appl. Opt. 42 (2003) 5744–5748.
[17] H. Nakanishi, H. Matsuda, S. Okada, et al., in: Proceedings of the Material Research Society International Meeting on Advanced Materials, vol. 1, Material Research Society, 1989, p. 97.
[18] S. Ohno, K. Miyamoto, H. Minamide, et al., Novel method to measure the refractive index and the absorption coefficient of organic nonlinear crystals in the ultra wideband THz region, in: The 34th International Conference on Infrared, Millimeter, and Terahertz Waves (IRMMW-THz 2009), 2009.
[19] H. Ito, K. Suizu, T. Yamashita, et al., Random frequency accessible broad tunable terahertz-wave source using phase-matched 4-dimethylamino-N-methyl-4-stilbazolium tosylate crystal, Jpn. J. Appl. Phys. 1 (46) (2007) 7321–7324.
[20] M. Ashida, R. Akai, H. Shimosato, et al., Ultrabroadband THz field detection beyond 170 THz with a photoconductive antenna, in: The Conference on Lasers and Electro-Optics (CLEO), CTuX6, 2008.
[21] W. Shi, Y.J. Ding, N. Fernelius, et al., Observation of difference-frequency generation by mixing of terahertz and near-infrared laser beams in a GaSe crystal, Appl. Phys. Lett. 88 (2006) 101101-1–101101-3.
[22] A.A. Babin, V.N. Petryakov, G.I. Freidman, Use of stimulated scattering by polaritons in detection of submillimeter radiation, Sov. J. Quant. Electron. 13 (1983) 958–960.
[23] R. Guo, S. Ohno, H. Minamide, et al., Highly sensitive coherent detection of terahertz waves at room temperature using a parametric process, Appl. Phys. Lett. 93 (2008) 021106.
[24] H. Minamide, J. Zhang, R. Guo, et al., Terahertz-wave detection using an organic DAST crystal covering ultra-wide frequency range at room temperature, in: Conference on Lasers and Electro Optics 2009, CLEO 2009, 2009.
[25] H. Minamide, J. Zhang, R. Guo, et al., Tunable terahertz-wave detection using a DAST optical up-conversion, in: The 34th International Conference on Infrared, Millimeter, and Terahertz Waves, IRMMW-THz 2009, 2009.
[26] T. Ikari, S. Aiba, H. Minamide, et al., Water content level mapping by THz wave in thin biological tissue, in: The 15th International Conference on Luminescence and Optical Spectroscopy of Condensed Matter, 2008, p. 268.
[27] S. Ohno, A. Hamano, K. Miyamoto, et al., Surface mapping of carrier density in a GaN wafer using a frequency-agile THz source, J. Europ. Opt. Soc. Rap. Public. 4 (2009) 09012.